Mechanical failure in amorphous solids: Scale-free spinodal criticality

Itamar Procaccia, Corrado Rainone, and Murari Singh
Department of Chemical Physics, the Weizmann Institute of Science, Rehovot 76100, Israel
(Received 17 April 2017; published 14 September 2017)

The mechanical failure of amorphous media is a ubiquitous phenomenon from material engineering to geology. It has been noticed for a long time that the phenomenon is "scale-free," indicating some type of criticality. In spite of attempts to invoke "Self-Organized Criticality," the physical origin of this criticality, and also its universal nature, being quite insensitive to the nature of microscopic interactions, remained elusive. Recently we proposed that the precise nature of this critical behavior is manifested by a spinodal point of a thermodynamic phase transition. Demonstrating this requires the introduction of an "order parameter" that is suitable for distinguishing between disordered amorphous systems. At the spinodal point there exists a divergent correlation length which is associated with the system-spanning instabilities (known also as shear bands) which are typical to the mechanical yield. The theory, the order parameter used and the correlation functions which exhibit the divergent correlation length are universal in nature and can be applied to any amorphous solid that undergoes mechanical yield. The phenomenon is seen at its sharpest in athermal systems, as is explained below; in this paper we extend the discussion also to thermal systems, showing that at sufficiently high temperatures the spinodal phenomenon is destroyed by thermal fluctuations.

DOI: 10.1103/PhysRevE.96.032907

I. INTRODUCTION

Mechanical failure of amorphous solids is an unwanted and often catastrophic event, occurring when enough strain and stress accumulate due to external loading. The phenomenon is ubiquitous in nature in the form of earthquakes due to tectonic activity and in material engineering due to shear or tensile strains. The phenomenon is known to be "scale-free" in the sense that the statistics of energy release on failure appears to have no typical scale, a characteristic that is exemplified by the Gutenberg-Richter law [1] in the geophysical context. Many authors commented that this scale-free nature indicates that material failure should be a critical phenomenon with power-law scaling, but until recently the precise origin and the actual character of this criticality remained unknown. in the late 1980s P. Bak and coworkers [2] offered the idea of "self-organized criticality" to explain the ubiquity of such scale-free statistics, but the correspondence to the microscopic structure of amorphous solids and the particle-scale mechanisms that are responsible for the phenomenon remained mysterious. Recently [3,4], the source of the criticality was revealed in the form of a spinodal criticality which appears to be quite universal in athermal conditions independently of the detailed microscopic interactions between the particles forming the amorphous solids. The aim of this paper is to review the pertinent features of this phenomenon and extend its exploration from athermal systems to amorphous solids at finite temperatures. Among other issues discussed below it will be shown that when the temperature becomes high enough the spinodal characteristics are destroyed by thermal fluctuations.

Solids are states of matter capable to respond elastically to a small externally applied shear deformation [5]. However, when the external strain grows the response of all solids becomes mixed with plastic deformations, and eventually they suffer a mechanical yield. In crystalline solids plasticity and yield involve defects and dislocations. In amorphous materials, such as molecular and colloidal glasses, foams, and granular matter, there is no long-range order with respect to which defects are defined. Thus the mechanisms of plasticity and yield need to be understood along different lines from those of crystalline matter. The physics near the yielding point of this vast class of materials, as reported in a host of strain-controlled simulations [6–12] and experiments [13–15] shows a high degree of universality despite the different nature of the systems involved. Importantly, one finds that at the onset of flow at yielding, there appear typical system spanning excitations referred to as shear bands [16,17]. We refer to a plastic event as a shear band when previously homogeneous shear strongly localizes, leaving the rest of the material less perturbed. This phenomenon is of capital importance for engineering applications as it is responsible for the brittleness typical of glassy materials, in particular metallic glasses [18], whose potential for practical use is stymied by their tendency to shear band and fracture [17,19,20]. Measurements of plastic events occurring after yield reveal scale-free energy or stress drops, typically characterized by power-law statistics [21,22]. The aim of this paper is to present the current understanding of this scale-free behavior which, as said above, is suspected to be related to some criticality.

In Sec. II we discuss the universal features of mechanical yield, explaining that any appropriate theory must use generic order parameters which are equally applicable to a large variety of amorphous solids. This is crucial. After discussing the order parameter, we turn to using the order parameter to investigate the physics of yield in athermal conditions. The key result will be that yield is tantamount to a spinodal point in the emerging phase transition that is associated with the phenomenon. In Sec. III we follow up on the identification of the precise criticality that is implied by the spinodal point and study the correlation functions that are expected to exhibit a divergent correlation length. We show in this section that the correlation length diverges as a power law in the distance from the spinodal point, cf. Eq. (17) below. Section V explores the modifications caused by having a finite temperature. Not too surprisingly, we will discover that at higher temperatures fluctuation destroy

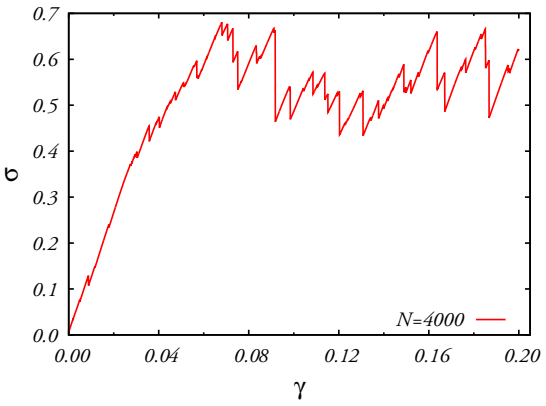

FIG. 1. A typical stress-vs.-strain curve resulting from a shear loading of an amorphous solids using an AQS protocol. Similar transitions between a regime in which the stress rises on the average as a function of strain to a second regime after a yield point γ_Y have been observed in countless experiments and simulations, requiring an explanation using a generic theory that is insensitive to microscopic details.

the spinodal characteristics, forcing a crossover to different statistics of the energy drops. In Sec. VI we offer a summary of the paper and thoughts about the road ahead.

II. MECHANICAL YIELD, UNIVERSALITY, AND ORDER PARAMETER

A. Universality of mechanical yield

To introduce the main issue, consider Fig. 1 showing a typical stress-vs.-strain curve obtained using standard numerical simulations in a strain-controlled athermal quasistatic (AQS) shearing protocol using a Kob-Andersen 65–35% Lennard-Jones (LJ) binary mixture [23] of 4000 particles in two dimensions (2D). The protocol is standard, and is implemented by increasing the shear strain on the system in small steps and after each such step apply gradient energy minimization to bring the system back to mechanical equilibrium. Similar curves were computed and measured in a large variety of simulations and experiments. The universal features that need to be observed are as follows: (i) For very small strain values the stress increases linearly according to the laws of linear elasticity. One should note that the region of purely elastic behavior is expected to reduce with the system size, shrinking to nonexistence in the thermodynamic limit. Nevertheless, before a value of the strain known as the "yield strain" γ_Y, the plastic events are "small," in the precise sense that the energy drop ΔU associated with them is system size independent,

$$\Delta U \sim N^0, \tag{1}$$

where N is the number of particles in the systems. The nature of these plastic events is identified as quadrupolar displacements, known also as Eshelby [24] events, which can release stress locally in regions that are particularly susceptible to the type of loading employed. The important thing is that, whether elastically or punctuated by plastic events, the stress σ continues to increase with the strain γ until the latter exceeds γ_Y, which in Fig. 1 is about $\gamma_Y \approx 0.07$. After that point, in strain-controlled protocols the strain increases without increasing the average stress—the material "flows," keeping an average "flow stress." In stress-controlled experiments, exceeding the average flow stress results in a mechanical collapse of the material. In athermal conditions it was found that the transition around $\gamma = \gamma_Y$ is associated with a change in the plastic response which is no longer localized but rather exhibits system spanning events, known also as micro shear bands, in which the energy release becomes subextensive [21],

$$\Delta U \sim N^\beta, \quad \beta = 2/3. \tag{2}$$

The mechanism for the creation of these micro shear bands was elucidated in Ref. [17]; it has to do with the preferred appearance of concatenated series of Eshelby quadrupoles [lines in 2D or embedded in a plane in 3D] that organize the displacement field to localize the shear on narrow lines or planes, respectively. The interested reader is referred to Ref. [19], where detailed energy estimates were offered to explain the energetic preference of single Eshelby quadrupoles at low strains vs the appearance of a density of such objects at higher values of the strain.

The key observation is that after yield strain γ_Y the stress cannot grow on average, no matter how much the strain is increased. What has long remained obscure is what the difference is in the material before and after the yield point, and why the stress could continue growing with the strain before yield, but it cannot do that after yield. Since the phenomenon is ubiquitous, the universality of this basic phenomenology of yielding begs an explanation in terms of a universal theory, in the sense that such a theory should rely on a statistical-mechanical framework and be independent of details such as chemical composition and the production process of the material.

B. Order parameter and transition

In Ref. [3] it was made clear that the difficulty in making a distinction between the pre- and postyield configurations lies in the fact that *there is really no distinction*. It is difficult to characterize a major change in the nature of configurations at yield. The important point is that there is a tremendous increase in the *number* of allowed configurations. The yield is tantamount to a sudden opening up of a vast number of marginally stable configurations that are not available to the system before yield. To demonstrate this one needs to employ an order parameter that is designed [25–32] to compare two different glassy configurations $\{\boldsymbol{r}_i^{(1)}\}_{i=1}^N$ and $\{\boldsymbol{r}_i^{(2)}\}_{i=1}^N$

$$Q_{12} \equiv \frac{1}{N}\sum_i^N \theta\big[a - \big|\boldsymbol{r}_i^{(1)} - \boldsymbol{r}_i^{(2)}\big|\big], \tag{3}$$

wherein $\theta(x)$ is the Heaviside step function. The parameter a is of the order of the microscopic interaction length and is determined by trial and error. The quantity Q_{12} is called an "overlap" since it has a value that goes from 0 (completely decorrelated configurations) to 1 (identical particle coordinates within the tolerance of a). Its purpose is to measure the degree of similarity between configurations.

The glass that we are straining below is made by quenching a supercooled liquid with N particles down to a certain temperature $T \geqslant 0$ at a suitable rate. A glass is an amorphous solid wherein particles vibrate around an amorphous structure. So if we take two configurations $\{\boldsymbol{r}_i^{(1)}\}_{i=1}^N$ and $\{\boldsymbol{r}_i^{(2)}\}_{i=1}^N$ from this glass at two different times, then they will be most likely close to each other with Q_{12} of the order of unity. By considering a sufficiently good sampling of the typical configurations visited by the particles in the glass, one can measure the probability distribution function (pdf) of the overlap $P(Q_{12})$. This pdf will be strongly peaked around an average value $\langle Q_{12}\rangle$ close to unity. The configurations visited by the particles will then form a small connected "patch" in the configuration space of the system, selected by the amorphous structure provided by the last configuration that was visited by the liquid glass former before it fell out of equilibrium while forming a glass.

Consider now what happens when we strain this glass. While the stress increases, there appear plastic events that are associated with irreversible displacements in the particle positions. The average order parameter $\langle Q_{12}\rangle(\gamma)$ responds to these displacements, reducing from $O(1)$ to lower values. An important point to understand is that before reaching the yield strain $\langle Q_{12}\rangle(\gamma)$ tends to remain around unity, but as the mechanical yield takes place a sharp phase transition occurs, where subextensive plastic events [11,17,20] begin to take place. These are sufficiently large, cf. Eq. (2), to cause substantial displacements, allowing different regions of the configuration space to affect the order parameter. In such a situation, the distribution $P_\gamma(Q_{12})$ may develop two peaks: one at high Q_{12} corresponding to configurations in the same patch and one for a smaller value of Q_{12} corresponding to configurations that were "ergodized" by the mixing of the subextensive plastic events. A visual of the system spanning event that ergodizes the system is available, for example, in Fig. 4 of Ref. [4].

To demonstrate this fundamental idea, we can use any model glass, since this order parameter description is expected to be universal. Here we review molecular dynamics simulations of a Kob-Andersen 65–35% LJ binary mixture in 2D, using five system sizes, $N = 500, 1000, 2000, 4000$, and $N = 10\,000$. We chose Q_{12} with $a = 0.3$ in LJ units but verified that changes in a leave the emerging picture invariant. As a first step, we prepared a glass by equilibrating the system at $T = 0.4$, and then quenching it (the rate is 10^{-6} in LJ units) down to $T = 1 \times 10^{-6}$ into a glassy configuration. The sample is then heated up again to $T = 0.2$, and a starting configuration of particle positions is chosen at this temperature. Note that while at $T = 0.4$ equilibration is sufficiently fast, at $T = 0.2$ the computation time is much shorter than the relaxation time. The configuration is then assigned a set of velocities randomly drawn from the Maxwell distribution at $T = 0.2$, and these different samples are then quenched down to $T = 0$ at a rate of 0.1. This procedure can be repeated any number of times (say, n times), and it allows us to get a sampling of the configurations inside one single "patch." We verify that the typical overlap of the ensemble of configurations so obtained in one patch is close to $\langle Q_{12}\rangle = 1$, signaling that indeed the ensemble is completely located in a single patch.

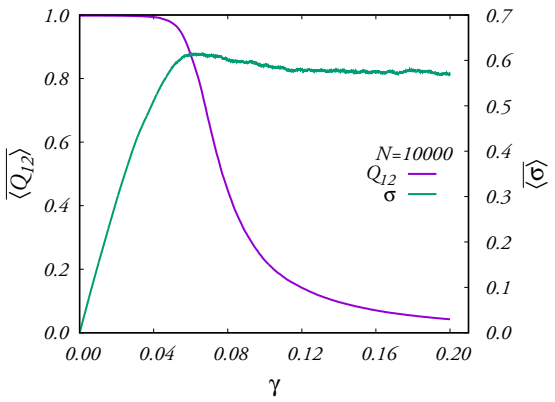

FIG. 2. The averaged order parameter $\overline{\langle Q_{12}\rangle}$ as a function of γ (left scale) and the averaged stress as a function of γ (right scale). The averaging is over all the patches for this systems size $N = 10\,000$. Note the phase transition that occurs near the yield stress. The transition gets sharper with the system size, see Fig. 6 and the associated discussion below.

Having generated one such patch, we repeat the procedure starting from another equilibrated configuration of the liquid to create another patch. The process is then repeated to generate as many patches (say m patches) as needed to obtain good statistics, depending on the system size.

We then apply to *each configuration* in a given patch an AQS protocol as described above. This will create for each value of γ a *strained ensemble* of configurations in the patch. The order parameter Eq. (3) is computed by using *all* the $n(n-1)/2$ unique pairs of configurations generated in the strained ensemble at a given γ. We stress that we do *not* compare configurations at a given value of γ to the reference configuration at $\gamma = 0$ but rather the overlap between pairs of configurations at the same value of γ. Having computed the γ dependence of an average $\langle Q_{12}\rangle$ from the $n(n-1)/2$ of configurations in one patch, we average the results over m patches to obtain the average order parameter denoted as $\overline{\langle Q_{12}\rangle}$, wherein the acute brackets denote the average over a single patch and the overline denotes the average over all patches. We present the results for $N = 10\,000$ in Fig. 2. Note that the initial ensemble for $\gamma = 0$ shows a value of the averaged order parameter $\overline{\langle Q_{12}\rangle} = 1$, signifying that our initial ensemble is indeed composed of close-by configurations. As the ensemble is strained, the value of the order parameter gets lower, dropping towards zero when the strain is increased beyond the yield strain. Below we will show that the sharpness of the transition depends on the system size N, getting sharper and sharper when N increases.

To determine the yield strain γ_y accurately, one should construct the probability distribution function (pdf) $P_\gamma(Q_{12})$ by hystogramming the values of Q_{12} within a patch of n configurations obtained as explained above, and then average the result over the m available patches. The result is denoted $\overline{P_\gamma(Q_{12})}$. We ask at which value of γ this averaged pdf has two equally high peaks, see Fig. 3. The resulting $\overline{P_\gamma(Q_{12})}$ determines a value of $\gamma_y \simeq 0.088$. Note that this criterion implies a sharp definition of "yield" which seems absent in the current literature. If accepted, it indicates that the mechanical

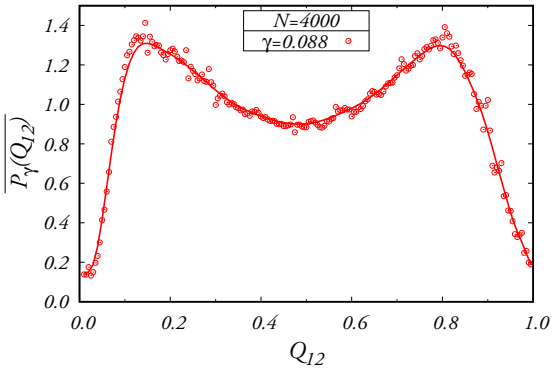

FIG. 3. The probability distribution function $\overline{P_\gamma(Q_{12})}$ at $\gamma_Y = 0.088$ averaged over 100 initial configurations each of which has 500 different realizations to obtain $\overline{P_\gamma(Q_{12})}$. At this value of the strain the pdf has two peaks of equal heights. We identify this value of γ as the point of the phase transition.

yield occurs beyond the stress overshoot in agreement with the mean-field results of Ref. [33]. We should also state here the yield point and the spinodal point (denoted below as γ_S) are not identical for finite N, although they become closer when N increases, and see below for details.

Having identified the phase transition point, we can examine the transition itself. In Fig. 4 we display the change in $\overline{P_\gamma(Q_{12})}$ in the neighborhood of the critical point γ_Y as a function of γ. Within a very narrow range of γ, of the order of $\Delta\gamma \approx 0.017$, we observe a first-order-like transition from a pdf with dominant peak at high values of Q_{12} to a dominant peak at low values of Q_{12}. We capture a very unambiguous and qualitative change in behavior as the yielding point is reached.

Next we can examime *how many* of our realizations loose the tight overlap and where the loss of overlap is taking place. To this aim we consider, as an example for the system of 4000 particles, all the 50 000 realizations that we have from 100 patches each containing 500 configurations. These are obtained by 100 choices of liquid realizations, each of which is velocity randomized 500 times (chosen with Boltzmann probabilities). When the strain γ is increased in our AQS algorithm, we keep computing the order parameter Q_{12} where the first configuration $\{\boldsymbol{r}_i^{(1)}\}_{i=1}^N$ in Eq. (3) is chosen randomly from all the available configurations at that value of γ, and the

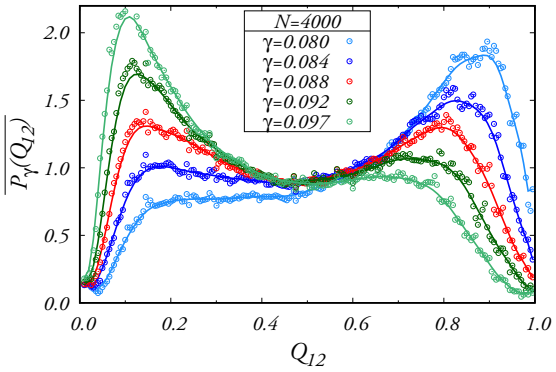

FIG. 4. The probability distribution function $\overline{P_\gamma(Q_{12})}$ in the vicinity of the critical point $\gamma_Y = 0.088$.

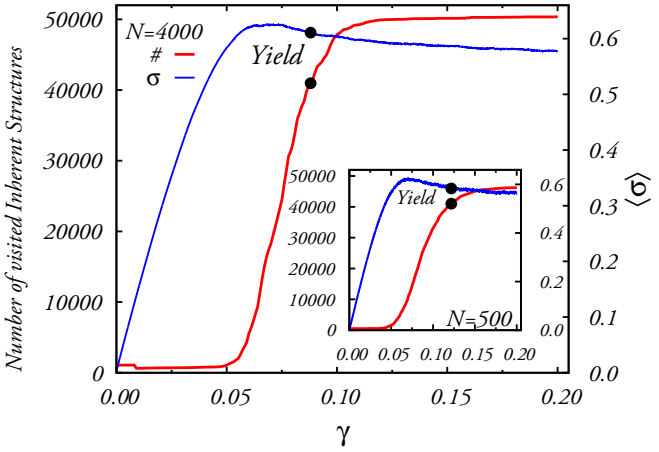

FIG. 5. The number of configurations which pass below the threshold value $Q_{12} = 0.8$ of the overlap order parameter as a function of the strain γ for $N = 4000$. In the inset we show the same test for $N = 500$. The conclusion is that *all the configurations* lose the mutual overlap in the vicinity of the yield point γ_Y.

second is any one of the other available configurations at the same value of γ. We confirmed that changing the randomly chosen $\{\boldsymbol{r}_i^{(1)}\}_{i=1}^N$ does not affect the results. Next, choosing $Q_{12} = 0.8$ as a threshold value, we now count how many of our observed configurations cross this threshold and exhibit $Q_{12} \leqslant 0.8$. The number of configurations that do so as a function of the strain (superimposed on the stress-vs.-strain curve) is shown in Fig. 5. The conclusion of this test is that in the vicinity of the yield point γ_Y *the majority of the configurations* lose their overlap with the initial configuration but *not before*. The mechanical yield is tantamount to the opening up of a vast number of possible configurations, whereas before yield the system is still constrained to reside in the initial metabasin of the free-energy landscape.

The upshot of these results is that we are able to focus on the essential feature that is responsible for the mechanical yield: a very constrained set of configurations available to the system before yield is replaced on yield with a vastly larger set of available configurations. This much larger set is generic; we would like to refer to the phenomenon as "stressed ergodization." The initially prepared close-by configurations are now scattered, but all of them are stressed with stress value close to the yield stress. They are all marginally stable in the sense that they would yield plastically with any increase of strain [34,35]. We propose this as a universal mechanism for the ubiquitous prevalence of stress-vs.-strain curves that look so similar in a huge variety of glassy systems.

C. System size dependence

In the context of first-order phase transitions, one expects that the transition should become sharper as a function of system size. To this aim we consider the dependence of $\overline{\langle Q_{12}\rangle}$ on γ for a series of system sizes, see Fig. 6. Indeed, the sharpening of the transition is obvious to the bare eye. To quantify it, we evaluated the derivative of this function, see the upper panel in Fig. 7 for $N = 4000$,

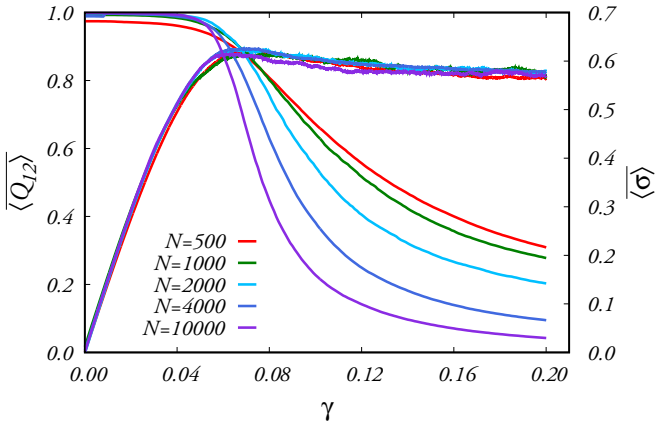

FIG. 6. Demonstrating the sharpening of the transition with the system size.

and computed the maximum of this derivative function, denoted as

$$S \equiv \max_{\gamma}\left(-\frac{d\overline{\langle Q_{12}\rangle}}{d\gamma}\right). \tag{4}$$

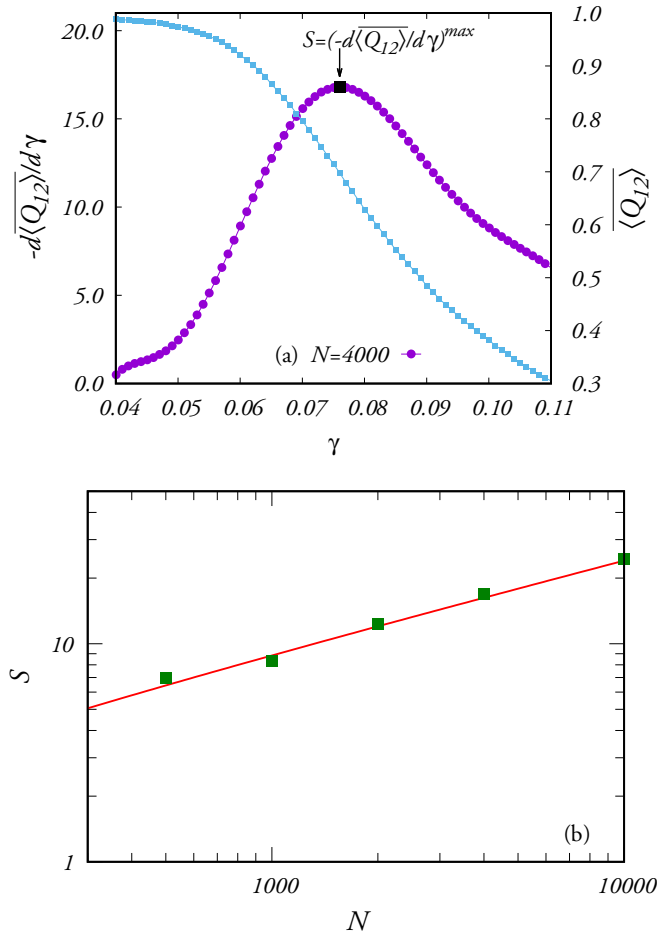

FIG. 7. Panel (a): A typical graph of $\overline{\langle Q_{12}\rangle}$ as a function of γ (here for $N = 4000$ (right scale) and the slope of the same function (left scale). Panel (b): The maximal slope of the function $\overline{\langle Q_{12}\rangle}(\gamma)$ as a function of system size.

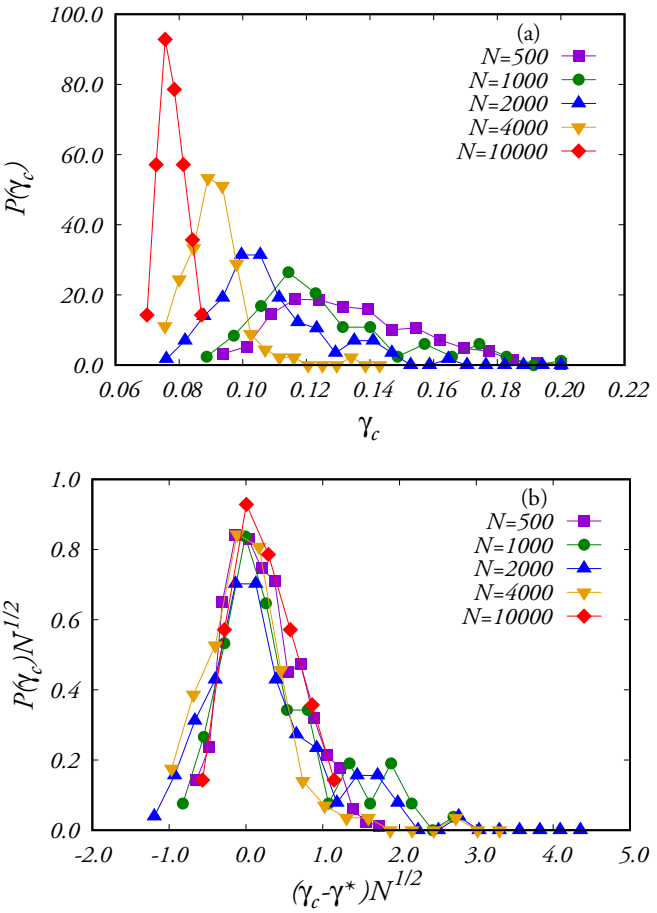

FIG. 8. Panel (a): The pdf's $P(\gamma_c, N)$ for different systems sizes from $N = 500$ to $N = 10\,000$. Panel (b): Data collapse on rescaling the pdf's $P(\gamma_c, N)$ according to Eq. (6) to obtain a scaling function $\tilde{P}(x)$ with $x = [(\gamma_c - \gamma^*)\sqrt{N}]$.

Finally, the value of $S(N)$ is plotted in a log-log plot vs. the system size N as shown in the lower panel of Fig. 7. This log-log plot indicates the existence of a power law of the form

$$S \approx CN^{\theta}\,; \theta = 0.41 \pm 0.09. \tag{5}$$

The error bars measured here is compatible with an exact value of the exponent θ is $\theta = 1/2$, and see below for a justification of this value. Such an exponent indicates that the width of the transition is not determined by the thermal fluctuations in the parent fluid from which our glassy patches were quenched. Rather, it is dominated by the disorder fluctuations which cause γ_Y to vary from sample to sample. To test this hypothesis, we return to our numerical data and compute, for each patch a yield point γ_c which we identify as the first value of the strain for which $\langle Q_{12}\rangle \leqslant 0.5$. Having done so, we can evaluate the probability distribution function $P(\gamma_c, N)$. These functions obviously depend on the systems size as shown in the upper panel of Fig. 8. To examine the scaling of the width of these distributions, we rescale the data according to the ansatz

$$P(\gamma_c, N) = \sqrt{N}\tilde{P}[(\gamma_c - \gamma^*)\sqrt{N}], \tag{6}$$

where γ^* is the peak value of each pdf. The data collapse means that, indeed, the disorder leads to a spread Δ_{γ_c} in the

values of γ_y that scales like

$$\Delta_{\gamma_c} \sim N^{-1/2}, \tag{7}$$

which will end up as the scaling law Eq. (5) with $\theta = 1/2$. If we just had a thermal origin to the measured width, then we could expect rather a scaling law with $\theta = 1$, as typical of first-order transitions [36].

D. Concluding this section

The upshot of this section is that the yield is associated with a first-order phase transition such that before yielding the amorphous system is limited to a small patch in the configuration space, very far from any kind of ergodicity. The yielding transition is an opening of a much larger available configuration space, whereupon the system is ergodized subject to the constraint of constant mean stress. The generic configurations that are created by the mixing caused by micro shear bands include many marginally stable states which yield easily on the increase of strain. This is why the stress cannot increase further on the average.

This realization does not explain yet where is the criticality. In general, first-order phase transitions are not characterized by diverging correlation lengths, while critical points associated with second-order phase transitions do. The point to understand, as sharpened in the next section, is that first-order phase transitions are bordered by spinodal points which do exhibit criticality. To see this pictorially, examine again Fig. 4 and focus on the pdf associated with $\gamma = 0.097$. At that point the maximum of high values of $\overline{\langle Q_{12}\rangle}$ has been reduced to a saddle. This is a spinodal point that we denote as γ_S where the slope of the curve vanishes as well as the second derivative. This is where a correlation length is expected to diverge as we are going to explain in the next section. The reader should also take into account that when $N \to \infty$ also $\gamma_c \to \gamma_S$.

III. THEORY OF SPINODAL CRITICALITY

The aim of this section is to clarify the identification of the yielding transition as a spinodal point [37]. This is the point where the metastable, high overlapped glassy patch of configurations becomes unstable with respect to a new phase with low Q_{12}, associated with a stressed ergodized system in the presence of disorder [38]. The existence of the spinodal point can be gleaned from Fig. 4. Observe the curve for $P(Q_{12})$ for $\gamma = 0.097$ where the right maximum flattens to a saddle with zero slope with respect to Q_{12}. This is the spinodal point γ_S. The appearance of shear bands will be associated with a system spanning correlation length, conditional that one is able to derive the expression of the right correlator to measure. It is important to stress here that the reason that a spinodal point can be exposed and measured is that the glassy time scales and the athermal conditions stabilize the metastable system until the spinodal point is crossed and the system becomes unstable against constrained ergodization. We will see below how thermal fluctuations may destroy the spinodal characteristics.

In statistical mechanics with a suitable Gibbs free energy $G[\phi]$, stable phases are identified with its points of minimum in ϕ. Of particular interest are instances for which the curvature of these minima goes to zero, inducing a critical behavior which manifests diverging susceptibilities and fluctuations, critical slowing down of the dynamics, and growing correlation lengths [39]. At a spinodal point, for example, one such minimum becomes unstable and transforms into a saddle. In the case of the order parameter Q_{12}, the general form of the free energy $s[Q_{12}]$ had been already derived and studied (see Ref. [40] for a review) in the context of the theory of replicas originally developed for the study of spin glasses, and its properties, at least at a mean-field level, are well known (we refer to Refs. [33,41] for the derivation of $s[Q_{12}]$ in the specific case of mean-field hard spheres); the matrix of second derivatives (or, using a more field-theoretic terminology, the mass matrix) is not diagonal in the basis of Q_{12} and after diagonalization is found to have only three distinct modes or masses [40]. Of these, the most relevant ones are the so-called *replicon mode* λ_R, which, for example, goes to zero at the newly proposed Gardner transition [42], and the *longitudinal mode* λ_L, which is instead related to spinodal points [37,41] such as our yielding transition. In Appendix of this paper we review briefly the background theory that is at the basis of the present approach.

A. Correlation functions

Based on the introductory discussion, we now derive an expression for the correlator associated with the longitudinal mode, from whence one can extract the diverging correlation length associated with the onset of criticality at the spinodal point and define an associated susceptibility which will shoot up as the spinodal point is approached. The first step is to "localize" the overlap function and define the $\boldsymbol{r}$-dependent quantity

$$Q_{12}(\boldsymbol{r}) \equiv \sum_{i=1}^{N} \theta\big(\ell - \big|\boldsymbol{r}_i^{(1)} - \boldsymbol{r}_i^{(2)}\big|\big)\delta\big(\boldsymbol{r} - \boldsymbol{r}_i^{(1)}\big). \tag{8}$$

Next, as mentioned above, the expression for the longitudinal correlator in terms of four-replica correlation functions can be found by diagonalization of the correlation matrix $G_{ab;cd}$ (see Appendix), which is defined as the inverse of the mass matrix $M_{ab;cd}$ of the replicated field theory of the overlap order parameter Q_{12} [40]. The derivation is a matter of standard diagonalization algebra, so we shall not report it here and refer to Appendix for the details. The expression, employed, for example, in Refs. [43,44] in the case of a model with spins on a lattice, reads for athermal systems

$$G_L(\boldsymbol{r}) = 2G_R(\boldsymbol{r}) - \Gamma_2(\boldsymbol{r}), \tag{9}$$

with the definitions

$$G_R(\boldsymbol{r}) \equiv \overline{\langle Q_{12}(r)Q_{12}(0)\rangle} - 2\overline{\langle Q_{12}(r)Q_{13}(0)\rangle} + \overline{\langle Q_{12}(r)\rangle\langle Q_{34}(0)\rangle}, \tag{10}$$

$$\Gamma_2(\boldsymbol{r}) \equiv \overline{\langle Q_{12}(\boldsymbol{r})Q_{12}(0)\rangle - \langle Q_{12}(\boldsymbol{r})\rangle\langle Q_{12}(0)\rangle}. \tag{11}$$

We reiterate that angular brackets denote a patch average and $\overline{(\bullet)}$ indicates an average over different patches. The quantity $G_R(\boldsymbol{r})$ is the correlation function of the replicon mode [40] and $\Gamma_2(\boldsymbol{r})$ is just the garden-variety four-point correlator.

Using these definitions and taking Eq. (8) into account, the quantities we compute in numerical simulation, before taking the ensemble average, are (see Appendix and Ref. [45])

$$\tilde{\Gamma}_2(\boldsymbol{r}) = \frac{\sum_{i\neq j}\left(u_i^{(12)} - Q_{12}\right)\left(u_j^{(12)} - Q_{12}\right)\delta\left[\boldsymbol{r} - \left(\boldsymbol{r}_i^{(1)} - \boldsymbol{r}_j^{(1)}\right)\right]}{\sum_{i\neq j}\delta\left[\boldsymbol{r} - \left(\boldsymbol{r}_i^{(1)} - \boldsymbol{r}_j^{(1)}\right)\right]} \tag{12}$$

and

$$\tilde{G}_R(\boldsymbol{r}) = \frac{\sum_{i\neq j}\left[u_i^{(12)}u_j^{(12)} - 2u_i^{(12)}u_j^{(13)} + Q_{12}Q_{34}\right]\delta\left[\boldsymbol{r} - \left(\boldsymbol{r}_i^{(1)} - \boldsymbol{r}_j^{(1)}\right)\right]}{\sum_{i\neq j}\delta\left[\boldsymbol{r} - \left(\boldsymbol{r}_i^{(1)} - \boldsymbol{r}_j^{(1)}\right)\right]}, \tag{13}$$

with

$$u_i^{(12)} \equiv \theta\left[\ell - \left|\boldsymbol{r}_i^{(1)} - \boldsymbol{r}_i^{(2)}\right|\right]. \tag{14}$$

These four-replica objects can be computed for any quadruplet of distinct replicas. The ensemble averaged correlation functions are simply obtained as $\Gamma_2 \equiv \overline{\tilde{\Gamma}_2^{(12)}}$ and $G_R \equiv \overline{\tilde{G}_R^{(12)}}$, and cf. Appendix for a proof. We stress that one must keep the full space dependence of the correlators in the definitions above, as the shear strain breaks the rotational symmetry of the glass samples and so the correlators are not just functions of a distance r.

IV. NUMERICAL RESULTS

The three correlation function discussed in the previous section were computed in the same numerical simulations discussed in Sec. II B. Typical results are shown in Fig. 9, here at $\gamma_S = 0.09405$. One notices the obvious fact that the correlation functions reflect the breaking of isotropy that is caused by the strain. In fact the structure of the correlation function is quadrupolar precisely indicating where shear bands are bound to appear in simple strain. The x and the y axes are in 45° to the principal axis of the stress [46].

To demonstrate the strain dependence of the correlators we consider first the susceptibilities χ_{G_L}, χ_{G_R}, and χ_{Γ_2} that can be obtained from the correlators. For example,

$$\chi_{G_L}(\gamma) \equiv \int d^2x\, G_L(x,y;\gamma). \tag{15}$$

In Fig. 10 (upper panel) we show the susceptibility χ_{Γ_2} as a function of γ for the three system sizes at our disposal. Superimposed are the stress-vs.-strain curves obtained by averaging the individual curves over all the available configurations and glass samples. One sees very clearly the singularity that develops near the spinodal point as a function of the system size. In the middle and lower panels of the same figure we show the other two susceptibilities χ_{G_R} and χ_{G_L} as a function of the strain γ, again with the stress-strain curve superimposed for comparison. As we expected, the susceptibilities show a distinct peak at the spinodal point γ_S where criticality is reached.

The scaling of the peak of the susceptibility χ_{Γ_2} with the system size is expected to mirror the scaling of the response as written in Eq. (4), at least if standard fluctuation-dissipation theorems should apply to the present problem. Indeed, plotting the maximal values of $-\chi_{\Gamma_2}$ as a function of N in a log-log plot, cf. Fig. 11, we find that the maxima $\chi_{\Gamma_2}^{\max}$ scale like $\sqrt{N}$ as expected.

More detailed information is provided by the full dependence of the correlators on their arguments. To see most clearly the change in the correlators as the spinodal point is approached, we consider, for example, the one-dimensional function $G_R(x = 0, y; \gamma)$, shown for $N = 4000$ in Fig. 12. We note that the correlator changes both in amplitude and in extent when we approach the critical point. To quantify these changes, we fit a three-parameter function to $G_R(x = 0, y)$ in the form

$$G_R(x = 0, y; \gamma) \approx C + A\exp(-y/\xi), \tag{16}$$

where all the fitting coefficients are functions of γ. In Fig. 13 we present the γ dependence of the amplitude $A(\gamma)$, the constant C, and the correlation length $\xi(\gamma)$.

An interesting observation concerns the constant C used in the fit [Eq. (16)]. This constant is also sensitive to the approach of the criticality, cf. the lower panel in Fig. 13. One could worry that integrating this constant over y could contribute to the divergence of the susceptibilities. In fact, the rise in C near the spinodal point goes down with the system size and its contribution to the integral is reduced as well, as can be seen in Fig. 14, which presents the integral $\int dy G_R(x = 0, y)$ from which $C \times L$ is subtracted. The conclusion is that indeed the contribution of C goes down also when integrated over the system size, showing that the main contribution to the divergence of the susceptibility is from the divergence of the correlation length. It is interesting to notice that the constant C decreases with the system size, presumably becoming irrelevant in the thermodynamic limit. The amplitude A is still increasing with the system size, and it is difficult to assert whether it converges or not. On the other hand, we can safely conclude that the data present strong evidence for the increase in the correlation length. This conclusion is substantiated below using the correlation function $\Gamma_2(x, y)$. Before doing so, we need to discuss the fitting procedure for the correlation function $G_R(x = 0, y)$. In Fig. 15 we show the full results for this correlation function for all the available values of γ and for two larger systems sizes at our disposal. One sees that the exponential decay that is used for the fit is only reliable up to the minima of the functions. The reason for the upward trend is the periodic boundary condition that reflects the correlations. To eliminate this spurious effect we presented in Fig. 12 the fit up to the minimum in the function. One should note, however, that the distance to the minimum increases with the system

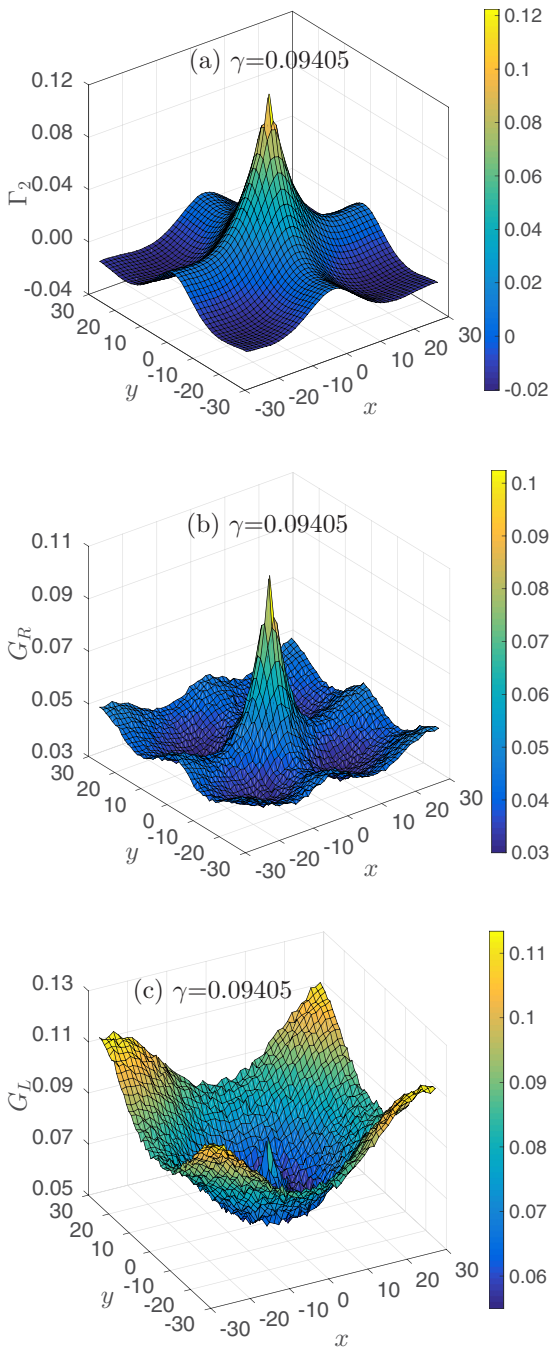

FIG. 9. A three-dimensional projection of the three correlation function as a function of x, y.

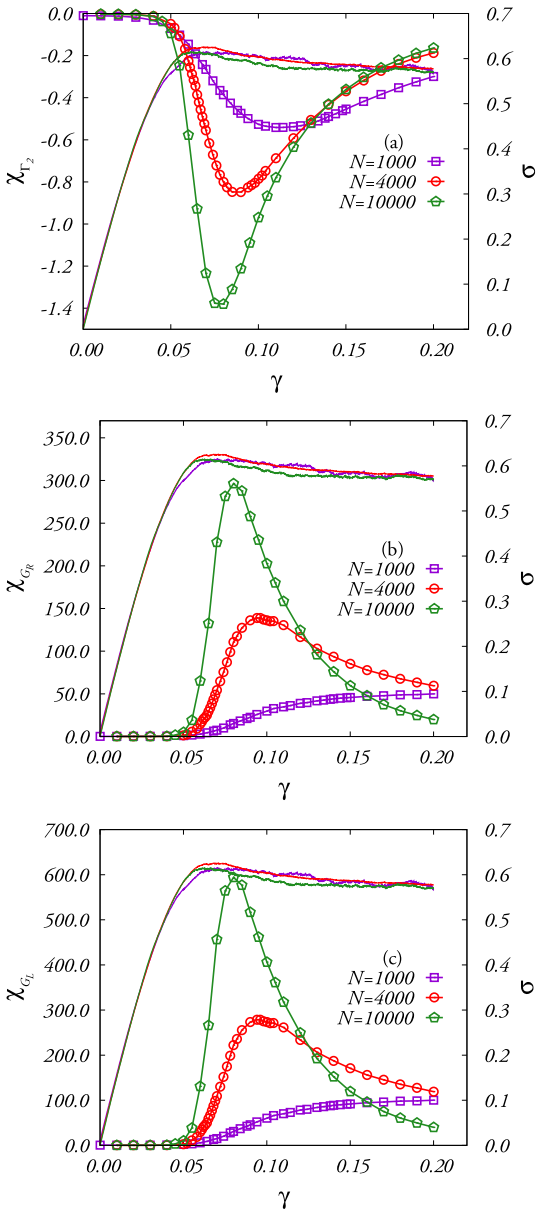

FIG. 10. The susceptibilities χ_{Γ_2} (a), and χ_{G_R} (b), and χ_{G_L} (c) as a function of γ for the three systems sizes available. Superimposed are the stress-vs.-strain curves for comparison. The color code is violet for $N = 1000$, red for 4000 and green for 10 000.

size, presumably diverging in the thermodynamic limit. Thus the fit up to the minimum allows a faithful estimate of the correlation length ξ.

The dependence of ξ on the distance from criticality and on the system size is not easy to read from Fig. 13. In fact, a smoother dependence is available from the correlation function $\Gamma_2(x = 0, y)$ and $\Gamma_2(y = 0, x)$. An exponential fit similar to Eq. (16) was applied to these two projections of $\Gamma_2(x, y)$ and the correlation length ξ was determined as shown in the upper panel of Fig. 16. The scaling exhibited in the lower panel of Fig. 16 is not perfect, but a least-squares fit to all the three curves leads to a scaling law in the form

$$\xi \approx (\gamma_c - \gamma)^{-\nu}, \quad \nu \approx 2.4 \pm 0.35. \tag{17}$$

The estimated value of ν is unusually high. The error bars are significant, and it is quite likely that this result is not incompatible with $\nu = 2$, although at the present time we cannot offer a theoretical basis for this number.

The result Eq. (17) may have important experimental consequences, predicting the length of microshear bands in materials as a function of the distance from criticality. We propose that such measurements should be carried out, providing a possible direct test of the present ideas.

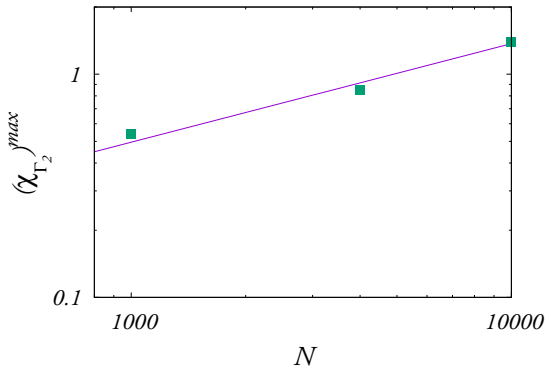

FIG. 11. The system size dependence of the maxima $\chi_{\Gamma_2}^{\max}$ indicating a dependence on $\sqrt{N}$ in correspondence to the results in Fig. 7.

V. THE EFFECTS OF FINITE TEMPERATURES

The mechanical yield in athermal conditions is an excellent conceptual laboratory for clarifying the essence of the yield mechanism, but in reality many yielding amorphous solids operate under thermal conditions, effected by thermal fluctuations. It is therefore interesting and important to assess the effects of temperature on the findings described above.

To assess the effects of temperature we repeat precisely the same protocol described above to create a patch of n replica at $T = 0$, including the creation of m such patches. The difference is that presently we warm up all the replica in a given patch to a target temperature. Results will be reported for target temperatures $T = 0.1, 0.2$. While keeping the strain at $\gamma = 0$, each configuration was thermalized by molecular dynamics. At that point each configuration was strained by increasing the strain in steps of $\delta\gamma = 2 \times 10^{-4}$, allowing the energy to stabilize after each such step before straining again. Typical averaged strain-vs.-stress curves (with averages computed first over a patch and second all the patches) for a system with $N = 10\,000$ are shown in the upper panel of Fig. 17. We see that at the lower temperature $T = 0.1$ there is still a stress peak before the yield, but at the higher temperature $T = 0.2$ the stress peak no longer exists and the stress reaches the flow steady-state stress quite monotonically. In both temperatures the steady state is attained at lower values of the strain than at $T = 0$. Computing the average overlap order parameters $\overline{\langle Q_{12}\rangle}$ (cf. lower panel of Fig. 17), we observe a corresponding behavior. At $T = 0.1$ a remnant phase transition is still observable, with the order parameter falling sharply after $\gamma \approx 0.04$. At $T = 0.2$ there is no longer a sharp decrease but rather a smooth decline of $\overline{\langle Q_{12}\rangle}$ as a function of γ. It is obvious that temperature fluctuations at $T = 0.2$ are sufficient to destroy the spinodal characteristic of our phase transition.

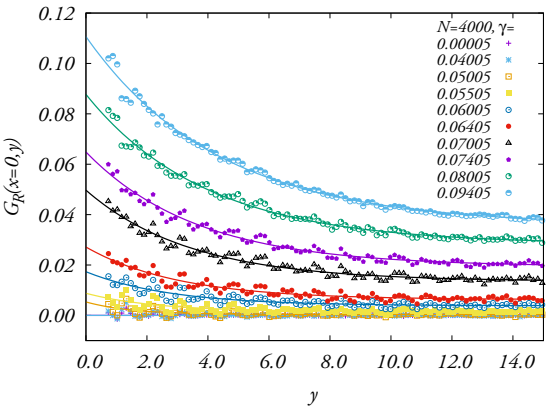

FIG. 12. The function $G_R(x = 0, y; \gamma)$ for various values of γ from 5×10^{-5} to 0.09405. Note the increase in the over all amplitude of the correlator as well as the increase in the correlation length. The lines through the data are the fit function Eq. (16).

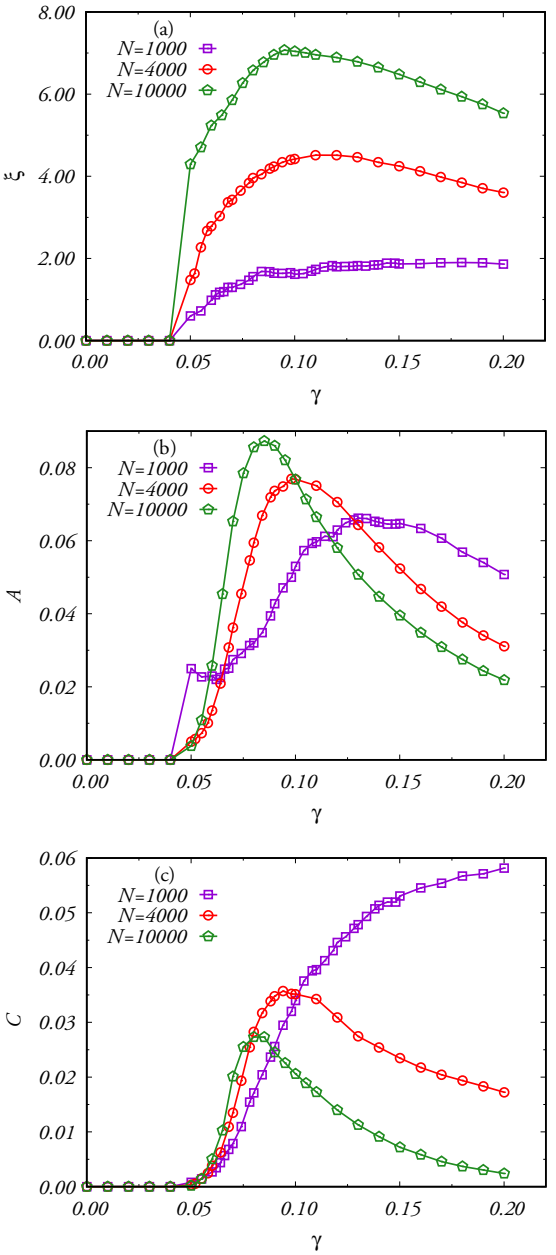

FIG. 13. The γ dependence of the correlation length $\xi(\gamma)$ (a), the amplitude $A(\gamma)$ (b) and the constant $C(\gamma)$ (c) in the best fit to the function $G_R(x = 0, y; \gamma)$, cf. Eq. (16).

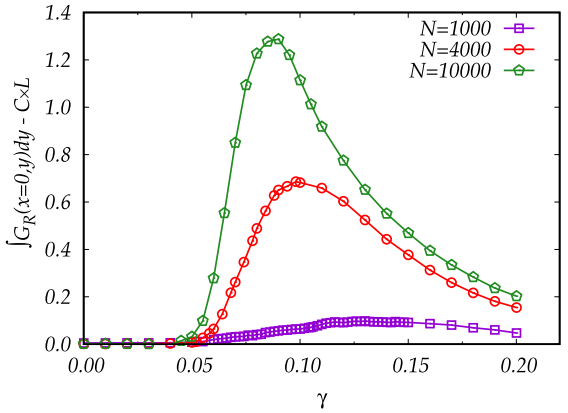

FIG. 14. The difference between $\int dy\, G_R(x=0,y)$ and $C \times L$.

The same conclusion is draws from examining the pdf of the order parameter. In Fig. 18 we show the function $\overline{P_\gamma(Q_{12},T)}$ for three temperatures $T = 0,0.1,0.2$ for a system with $N = 10\,000$. While the phase transition is observed nice and clear at $T = 0$, it still remains observable at $T = 0.1$, but it changes to a smooth migration of the single peak of $\overline{P_\gamma(Q_{12},T)}$ from high to low values of Q_{12} when γ is increased. We lose completely the double hump structure which underlies the spinodal criticality.

It is important to stress that with the loss of the spinodal criticality we also lose the qualitative distinction between the

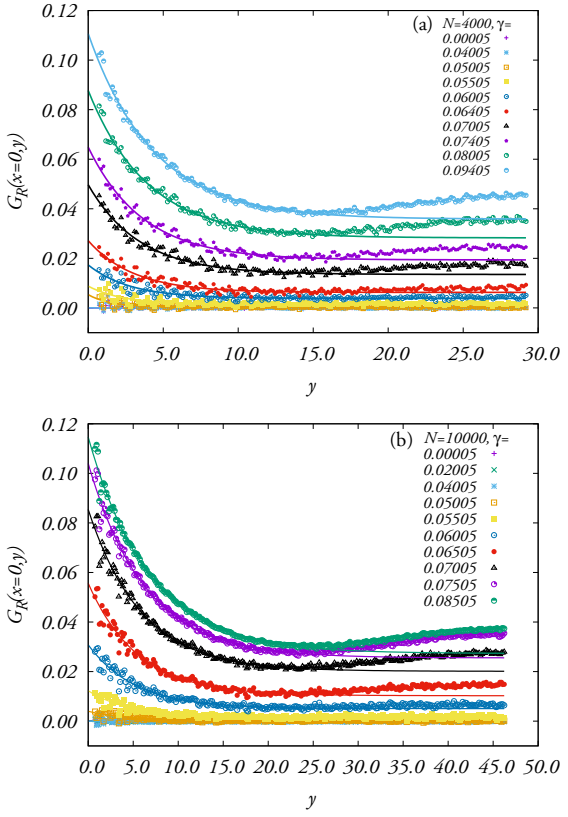

FIG. 15. The full y dependence of $G_R(x=0,y)$. The region fitted by Eq. (10) in the paper is shown. Note that the minimum in the function resides in higher values of y for larger system sizes.

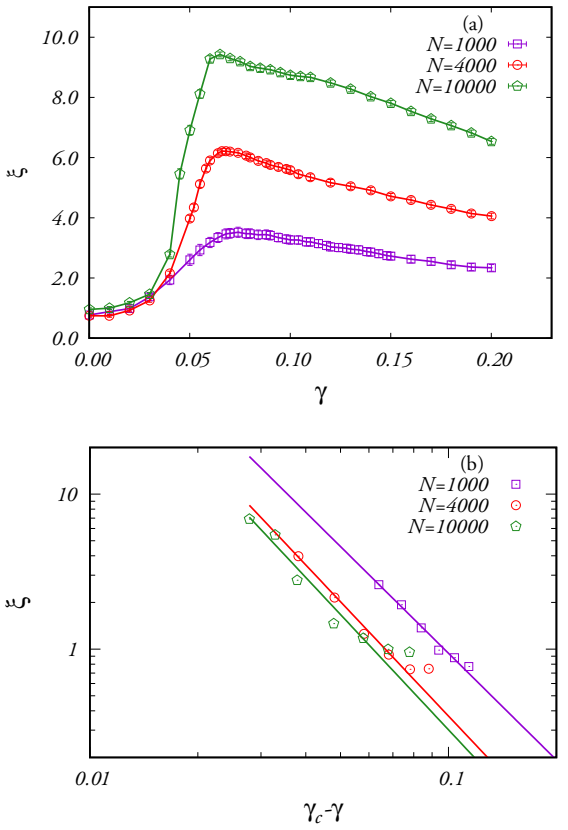

FIG. 16. Panel (a): The correlation length ξ read from an exponential fit to the x and y projection of the correlation function $\Gamma_2(x,y)$ for three values of the system size. Panel (b): The dependence of the correlation length ξ on $\gamma - \gamma_c$.

preyield and postyield statistics of the energy drops as shown in Eqs. (1) and (2). Observing a stress-vs.-strain curve for a single realization one finds the same statistics of energy and stress fluctuations before and after the yield. The sharp appearance of system spanning events with the yield phenomenon is caused by the spinodal criticality as explained in this paper. Once this get destabilized by temperature fluctuations there is no increase in correlation length and we remain with only standard temperature fluctuations.

This observation raises the question whether the mechanism of spinodal criticality could be observed in laboratory experiments where the temperature is finite. Clearly, one must choose materials that can be studied at temperatures that are much lower than the glass transition temperature T_g. For temperatures $T \ll T_g$ diffusion from cages is much suppressed even under strain. In such a situation we expect that the essence of the phenomenon discussed in this paper should be observed and shear bands should be visible and distinguishable from preyield plastic events. This point of view is corroborated by the observation of Ref. [47].

VI. SUMMARY AND CONCLUSIONS

In summary, we have presented evidence that the scale-free yielding transition in amorphous solids is governed by a spinodal point with disorder. The associated correlated length is exhibited by suitable four-point correlators whose

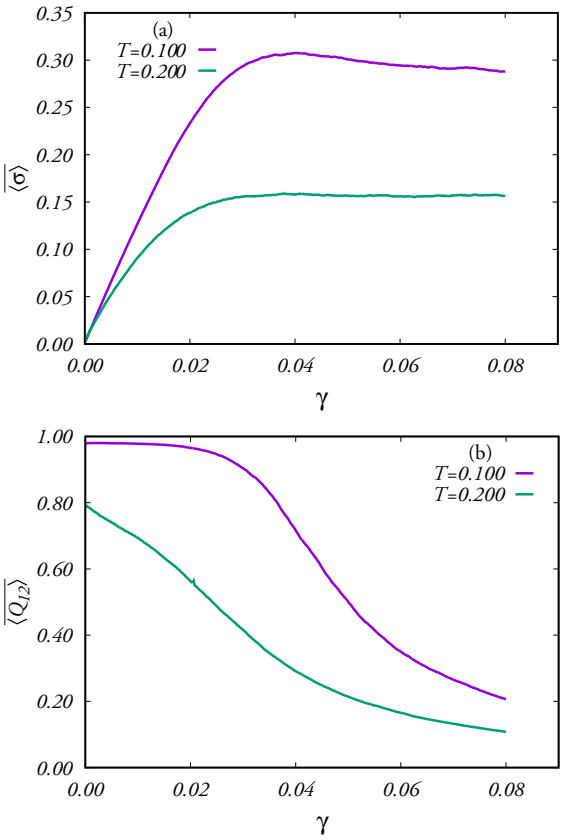

FIG. 17. Panel (a): Average stress vs. strain in quasistatic straining at finite temperature. The average is computed over all the configurations in a patch and then over the patches. Panel (b): The averaged overlap order parameter computed at the designated temperatures as a function of the strain γ. Here $N = 10\,000$.

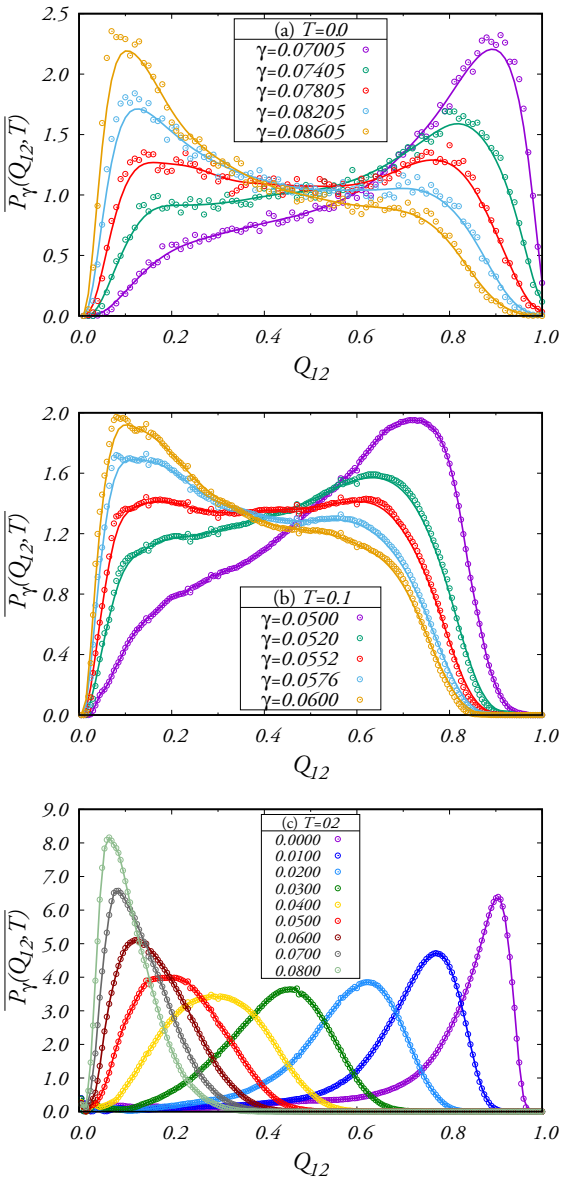

FIG. 18. The dependence of $\overline{P_\gamma(Q_{12},T)}$ on γ for three different temperatures $T = 0,0.1,0.2$.

expression can be obtained from replica theory. The full implications of the theory pertain to an athermal setting, and the full fledged criticality is destroyed by thermal fluctuations [47]. In athermal conditions the transition becomes ever sharper with increasing the system size. We have found that the range of strain values over which the transition takes place goes to zero like $1/\sqrt{N}$. The correlation length ξ appears to diverge a scaling law, cf. Eq. (17). We have commented above that this prediction may be tested experimentally by examining the lengths of micro shear bands as a function of the strain or the stress while approaching mechanical collapse. A previously known example of such a spinodal is the mode coupling theory transition [16], characterized by dynamical slowing down and heterogeneities, whose behavior is characterized by a *dynamical length scale* which can be extracted from suitable multipoint correlators [16]. Within replica theory, mode coupling theory corresponds to a spinodal point like it does in the present case of yielding; also in that case one can define susceptibilities that peak at the onset of the transition and which are associated with dynamical heterogeneities whose length scale grows on approaching the transition. The difference is that in mode coupling we have finite temperature so these excitations are transient in nature. Also in our present case, for sufficiently high temperatures the system will generally be able to escape through thermal activation from the high-Q_{12} minimum before this has a chance to flatten and the relative susceptibility to diverge. However, since the nucleation time is expected to be fairly long, one should anyway be able to observe *transient* shear-bands or heterogeneities, as long as the temperature is low enough that nucleation does not take place until the system is close to the spinodal, which, interestingly, is precisely the behavior of transient shear bands as reported in Ref. [47].

In the future, one needs to examine further the universality of the proposed scenario and of the scaling laws found in this paper, examining different amorphous systems and different space dimensionalities. Another interesting future path is the study of the mechanical yield in frictional aggregates. It is now known at the present point in time whether these fall in the same universality class or whether they might exhibit totally different behavior.

ACKNOWLEDGMENTS

We thank G. Parisi for inspiring discussions. We acknowledge interesting exchanges with G. Biroli regarding the effect of disorder on the width of the transition. I.P. was supported in part by the Minerva Foundation (Grant No. 712280) with funding from the Federal German Ministry for Education and Research and by the Israel Science Foundation (Israel Singapore Program) under Grant No. 2293/16.

APPENDIX: THE LONGITUDINAL CORRELATION FUNCTION

Let us start from the expression of the free energy of a glass state, prepared by equilibrating a generic glass former down to a glass transition temperature T_g where it can still be equilibrated, and then quenching it out of equilibrium to a given temperature $T < T_g$. Such a free energy was first defined in Ref. [25] in the context of spin-glass physics. Its definition in the case of structural glasses, and its computation in the particular case of hard spheres were first discussed in Ref. [33]. The definition, in the case of a generic glass former made of N particles is based on comparing two configurations X^a and X^b of the same glass. Here

$$X^a \equiv \{\boldsymbol{r}_i^a\}_{i=1}^N, \quad X^b \equiv \{\boldsymbol{r}_i^b\}_{i=1}^N, \tag{A1}$$

where the labeling $\boldsymbol{r}_i$ refers to the position of the same particle i in the two different configurations. For a generic interaction potential $V(X)$ the definition of the free energy is

$$f[T,T_g] \equiv -\frac{1}{\beta N}\int dX_0\,\frac{e^{-\beta_g V(X_0)}}{Z_g} \times \log\left[\int dX_1\, e^{\beta V(X_1)}\delta(q_r^* - Q_{01})\right], \tag{A2}$$

where $\beta_g = 1/(k_B T_g)$, $\beta = 1/(k_B T)$, and q_r^* is the value of $q_r \neq 0$ where the free energy attains a local minimum [33]. The overlap function Q_{01} for any two configurations, say, a and b, is [3]

$$Q_{ab} = \frac{1}{N}\sum_{i=1}^N \theta\left(\ell - \left|\boldsymbol{r}_i^a - \boldsymbol{r}_i^b\right|\right). \tag{A3}$$

Here ℓ is a coarse-graining parameter (in Ref. [3], $\ell \simeq 0.3$ in Lennard-Jones units). The idea is to consider the free energy at temperature T of the glass former, which is *constrained* to stay close to an amorphous configuration X_0 which is selected from the equilibrium ensemble, using the canonical distribution when the glass is still at equilibrium at T_g.

The properties and computation of the free energy (A2) are discussed extensively in [33,41], so we refer the interested reader to those works. The explicit analytic computation is accomplished in the mean-field approximation. In our paper we use the results far from the mean-field limit, but we ascertain that the relevant correlation functions that are fleshed out in the mean-field calculation are the relevant ones also in the general case. Of course, critical exponents can differ. In the sequel we sketch how from this mean-field theory in terms of an overlap order parameter Q_{ab} one can extract the definitions of the correlation functions that are expected to show critical behavior.

The outermost integral in the Eq. (A2) can be computed with the replica trick,

$$f[T,T_g] = \lim_{s\to 0}\partial_s \Phi[T,T_g;s], \tag{A4}$$

where Φ is defined as

$$\Phi[T,T_g;s] = -\frac{1}{\beta N}\log\int dX_0\, dX_1\cdots dX_s e^{-\beta_g V(X_0)} \times e^{-\beta V(X_1)}\delta(q - Q_{01})\cdots e^{-\beta V(X^s)}\delta(q - Q_{0s}), \tag{A5}$$

so we are considering s replicas of the X configuration. In infinite dimensions for the case of hard spheres it was shown [48] that the functional defined above can be written as

$$\Phi = -\frac{1}{\beta N}\int \mathcal{D}Q_{ab}\, e^{-dS(Q_{ab})}. \tag{A6}$$

Here $\mathcal{D}Q_{ab}$ denotes an integration measure over all the distinct Q_{ab}s,

$$\mathcal{D}Q_{ab} \equiv \prod_{a<b}^{0,s} dQ_{ab}, \tag{A7}$$

and d is the number of spatial dimensions. The functional $S(Q_{ab})$ is referred to as the "replica action." In the mean-field limit $d\to\infty$, the integral above can be computed via the saddle-point method [49], which means that one must consider the optimum points in Q_{ab} of the replica action $S(Q_{ab})$. This means that $S(Q_{ab})$ plays the role of a *Gibbs free energy*, i.e., the free energy for fixed order parameter. An illustrative example is the case of a Curie-Weiss model (mean-field ferromagnet) wherein, for the Helmholtz free energy F in zero magnetic field, one has [50]

$$F(h=0,T) = \min_m G(m,T), \tag{A8}$$

where $G(m,T)$ is indeed the Gibbs free energy for fixed magnetization m. The minimization equation for G is then the celebrated equation for the spontaneous magnetization

$$\frac{\partial G}{\partial m} = 0 \Longrightarrow m = \tanh(\beta m) \tag{A9}$$

and the ferromagnetic phase transition takes place when the paramagnetic, $m=0$ minimum of G flattens and splits in two degenerate minima with $m\neq 0$, which implies that at the critical temperature $\frac{\partial^2 G}{\partial m^2} = 0$. The derivation of the $S(Q_{ab})$ action in the case of mean-field hard spheres can be found in Ref. [48].

In the present case the $f[T,T_g]$ plays the role of the Helmholtz free energy F and the $S(Q_{ab})$ of the Gibbs free energy G. With this analogy, one can understand how the critical properties of glass states are related to the matrix of second derivatives of the replica action $S(Q_{ab})$,

$$M_{ab;cd} \equiv \frac{\partial^2 S}{\partial Q_{a<b}\partial Q_{c<d}}, \qquad a,b,c,d \in [1,s], \tag{A10}$$

in the limit $s\to 0$ (we stress that X_0 is not involved in this definition). The inverse $G_{ab;cd}$ of the tensor M, defined as

$$\sum_{e\neq f} M_{ab;ef}G_{ef;cd} = \frac{\delta_{13}\delta_{bd} + \delta_{ad}\delta_{bc}}{2} \tag{A11}$$

is then the covariance matrix of the mean-field theory

$$G_{ab;cd} = \overline{\langle (Q_{ab} - \langle Q_{ab}\rangle)(Q_{cd} - \langle Q_{cd}\rangle)\rangle}, \tag{A12}$$

wherein the angled brackets denote the thermal average restricted to a single glass sample at temperature T [that is over the canonical distribution of the X_1 configuration in the (A2)], and the overbar denotes the average over all possible glass samples selected at T_g [that is, over the canonical distribution of the X_0 configuration in the (A2)]. This covariance tensor encodes the critical fluctuations of the system near the critical points where the tensor $M_{ab;cd}$ develops a zero mode.

Let us now assume that the glass state under study is a single minimum of the free-energy landscape of the system wherein all replicas from 1 to s can move ergodically, this means that the replicas are all equivalent and the matrix Q_{ab} must then be invariant by any replica permutation, a hypothesis referred so as replica symmetric (RS).

In Ref. [33] it is discussed how this is not true in all cases, i.e., there exist a regime wherein the glass basin undergoes an ergodicity breaking and fractures into sub-basins. Nevertheless, here we stick to the simple RS ansatz. In this case, since the action $S(Q_{ab})$ must in turn be invariant for any replica permutations, the most general form that the Hessian M can take is

$$M_{ab;cd} = M_1\left(\frac{\delta_{ac}\delta_{bd} + \delta_{ad}\delta_{bc}}{2}\right) + M_2\left(\frac{\delta_{13} + \delta_{bd} + \delta_{ad} + \delta_{bc}}{4}\right) + M_3, \tag{A13}$$

and the same goes for the covariance matrix $G_{ab;cd}$. This form is completely general as it only pertains to the RS symmetry; then the only model dependence is in the parameters M_1, M_2, and M_3, which must be computed case by case and are generally dependent on the external parameters like temperature or magnetic field.

The diagonalization of the tensor $M_{ab;cd}$ is an exercise of standard linear algebra and has been already carried out many times, see, for example, Refs. [40,51–53] where it is proposed as an exercise. It is found that the tensor M has only three distinct eigenvalues

$$\lambda_R = M_1, \tag{A14}$$

$$\lambda_L = M_1 + (s-1)(M_2 + sM_3), \tag{A15}$$

$$\lambda_A = M_1 + \frac{s-2}{2}M_2, \tag{A16}$$

and the same goes for the tensor G. Those three eigenvalues (or modes) are called the *replicon*, *longitudinal*, and *anomalous*, respectively [53]. We are interested in the longitudinal mode (which in the limit $s \to 0$ is degenerate with the anomalous one), which becomes soft at the yielding transition [37,41]. Let us consider the G tensor. Because of replica symmetry, there are only three distinct correlators that one can define, namely

$$G_{12;12} = \frac{G_1}{2} + \frac{G_2}{2} + G_3, \tag{A17}$$

$$G_{12;13} = \frac{G_2}{4} + G_3, \tag{A18}$$

$$G_{12;34} = G_3, \tag{A19}$$

and in the limit $s \to 0$ we know that

$$\frac{1}{\lambda_L} = G_1 - G_2. \tag{A20}$$

It is then immediate to check that

$$G_{12;12} - 2G_{12;13} + G_{12;34} = \frac{G_1}{2} \propto \frac{1}{\lambda_R} \equiv G_R, \tag{A21}$$

$$G_{12;12} - 4G_{12;13} + 3G_{12;34} = \frac{G_1 - G_2}{2} \propto \frac{1}{\lambda_L} \equiv G_L, \tag{A22}$$

which then implies

$$G_L(\boldsymbol{r}) = 2G_R(\boldsymbol{r}) - \Gamma_2(\boldsymbol{r}), \tag{A23}$$

with the definitions

$$G_R(\boldsymbol{r}) \equiv \overline{\langle Q_{ab}(r)Q_{ab}(0)\rangle} - 2\overline{\langle Q_{ab}(r)Q_{ac}(0)\rangle} + \overline{\langle Q_{ab}(r)\rangle\langle Q_{cd}(0)\rangle}, \tag{A24}$$

$$\Gamma_2(\boldsymbol{r}) \equiv \overline{\langle Q_{ab}(\boldsymbol{r})Q_{ab}(0)\rangle} - \overline{\langle Q_{ab}(\boldsymbol{r})\rangle\langle Q_{ab}(0)\rangle}, \tag{A25}$$

as in the main text. We have used $\Gamma_2 = G_{12;12} - G_{12;34}$ which derives from replica symmetry, as $\langle Q_{12}\rangle\langle Q_{12}\rangle = \langle Q_{12}Q_{34}\rangle$ in the replica-symmetric phase.

Let us now detail how to transform these definitions into quantities that can be measured in simulation. We start by "localizing" the definition of the Q_{ab} overlap in the following way:

$$Q_{ab}(\boldsymbol{r}) \equiv \sum_{i=1}^{N} \theta\left(\ell - \left|\boldsymbol{r}_i^a - \boldsymbol{r}_i^b\right|\right)\delta\left(\boldsymbol{r} - \boldsymbol{r}_i^a\right). \tag{A26}$$

In a thermal simulation the a and b configurations would depend on the time t, and so would the $Q_{ab}(r)$, so one would need to perform the in-state thermal average $\langle\bullet\rangle$ by considering the equilibrium value of these quantities. In the present paper we focus on athermal solids under quasistatic shear, so we do not have dynamics and the a and b configurations will simply be two distinct minima of the interparticle potential obtained through the protocol described in the main text, and the thermal average will be the average over this ensemble of configurations which make up a glassy patch.

We now apply the definition (A26) in (A24) and (A25) to construct the correlators. For illustrative purposes, we use the $\Gamma_2(\boldsymbol{r})$. We get, omitting the overline to lighten the notation,

$$\langle [Q_{ab}(\boldsymbol{x}) - \langle Q_{ab}(\boldsymbol{x})\rangle][Q_{ab}(\boldsymbol{x}+\boldsymbol{r}) - \langle Q_{ab}(\boldsymbol{x}+\boldsymbol{r})\rangle]\rangle = \sum_{ij}\left[\left(u_i^{ab} - Q_{ab}\right)\left(u_j^{ab} - Q_{ab}\right)\right]\delta\left(\boldsymbol{r} + \boldsymbol{x} - \boldsymbol{r}_i^a\right)\delta\left(\boldsymbol{x} - \boldsymbol{r}_j^a\right), \tag{A27}$$

with

$$u_i^{ab} \equiv \theta\left(\ell - \left|\boldsymbol{r}_i^a - \boldsymbol{r}_i^b\right|\right), \tag{A28}$$

as in the main text, and we used that $\langle Q_{ab}(x)\rangle = Q_{ab}$. Because of translational invariance, the correlator is actually

independent of $\boldsymbol{x}$. We can get rid of $\boldsymbol{x}$ by performing an integration over this variable, which, using the δ functions, gives as a result

$$\sum_{ij}\left[\left(u_i^{ab}-Q_{ab}\right)\left(u_j^{ab}-Q_{ab}\right)\right]\delta\left[\boldsymbol{r}-\left(\boldsymbol{r}_i^a-\boldsymbol{r}_j^a\right)\right], \quad \text{(A29)}$$

then, following Ref. [45], we omit the terms with $i=j$ (which are anyway relevant only for $\boldsymbol{r}=0$) and we normalize the correlator with the pair distribution function of the glass; we finally obtain

$$\frac{\sum_{i\neq j}\left(u_i^{ab}-Q_{ab}\right)\left(u_j^{ab}-Q_{ab}\right)\delta\left[\boldsymbol{r}-\left(\boldsymbol{r}_i^a-\boldsymbol{r}_j^a\right)\right]}{\sum_{i\neq j}\delta\left[\boldsymbol{r}-\left(\boldsymbol{r}_i^a-\boldsymbol{r}_j^a\right)\right]}\equiv\tilde{\Gamma}_2(\boldsymbol{r}), \quad \text{(A30)}$$

as in the main text. The derivation for the $\tilde{G}_R(\boldsymbol{x})$ is then an obvious generalization.

[1] B. Gutenberg, *Seismicity of the Earth and Associated Phenomena* (Read Books Ltd, Redditch, UK, 2013).
[2] P. Bak, C. Tang, and K. Wiesenfeld, Phys. Rev. Lett. **59**, 381 (1987).
[3] P. K. Jaiswal, I. Procaccia, C. Rainone, and M. Singh, Phys. Rev. Lett. **116**, 085501 (2016).
[4] G. Parisi, I. Procaccia, C. Rainone, and M. Singh, Proc. Natl. Acad. Sci. USA **114**, 5577 (2017).
[5] L. D. Landau and E. M. Lifshitz, *Course of Theoretical Physics Vol 7: Theory of Elasticity* (Pergamon Press, London, 1959).
[6] F. Varnik, L. Bocquet, and J.-L. Barrat, J. Chem. Phys. **120**, 2788 (2004).
[7] C. Maloney and A. Lemaître, Phys. Rev. Lett. **93**, 016001 (2004).
[8] M. J. Demkowicz and A. S. Argon, Phys. Rev. B **72**, 245205 (2005).
[9] A. Tanguy, F. Leonforte, and J.-L. Barrat, Eur. Phys. J. E **20**, 355 (2006).
[10] A. Lemaître and C. Maloney, J. Stat. Phys. **123**, 415 (2006).
[11] E. Lerner and I. Procaccia, Phys. Rev. E **79**, 066109 (2009).
[12] D. Rodney, A. Tanguy, and D. Vandembroucq, Modell. Simul. Mater. Sci. Eng. **19**, 083001 (2011).
[13] G. Subhash, Q. Liu, and X.-L. Gao, Int. J. Impact Eng. **32**, 1113 (2006).
[14] A. Kara, A. Tasdemirci, and M. Guden, Mater. Des. **49**, 566 (2013).
[15] A. L. Noradila, Z. Sajuri, J. Syarif, Y. Miyashita, and Y. Mutoh, IOP Conf. Ser.: Mater. Sci. Eng. **46**, 012031 (2013).
[16] L. Berthier and G. Biroli, Rev. Mod. Phys. **83**, 587 (2011).
[17] R. Dasgupta, H. G. E. Hentschel, and I. Procaccia, Phys. Rev. Lett. **109**, 255502 (2012).
[18] M. Ashby and A. Greer, Scr. Mater. **54**, 321 (2006).
[19] R. Dasgupta, H. G. E. Hentschel, and I. Procaccia, Phys. Rev. E **87**, 022810 (2013).
[20] R. Dasgupta, O. Gendelman, P. Mishra, I. Procaccia, and C. A. B. Z. Shor, Phys. Rev. E **88**, 032401 (2013).
[21] S. Karmakar, E. Lerner, and I. Procaccia, Phys. Rev. E **82**, 055103(R) (2010).
[22] S. Franz and S. Spigler, Phys. Rev. E **95**, 022139 (2017).
[23] W. Kob and H. C. Andersen, Phys. Rev. Lett. **73**, 1376 (1994).
[24] J. D. Eshelby, Proc. Roy. Soc. Lond. A **241**, 376 (1957).
[25] S. Franz and G. Parisi, J. Phys. I France **5**, 1401 (1995).
[26] C. Cammarota, A. Cavagna, I. Giardina, G. Gradenigo, T. S. Grigera, G. Parisi, and P. Verrocchio, Phys. Rev. Lett. **105**, 055703 (2010).
[27] J. Yeo and M. A. Moore, Phys. Rev. E **86**, 052501 (2012).
[28] L. Berthier, Phys. Rev. E **88**, 022313 (2013).
[29] L. Berthier and D. Coslovich, Proc. Natl. Acad. Sci. USA **111**, 11668 (2014).
[30] G. Biroli, C. Cammarota, G. Tarjus, and M. Tarzia, Phys. Rev. Lett. **112**, 175701 (2014).
[31] L. Berthier and R. L. Jack, Phys. Rev. Lett. **114**, 205701 (2015).
[32] A. Ninarello, L. Berthier, and D. Coslovich, Mol. Phys. **113**, 2707 (2015).
[33] C. Rainone, P. Urbani, H. Yoshino, and F. Zamponi, Phys. Rev. Lett. **114**, 015701 (2015).
[34] S. Karmakar, E. Lerner, and I. Procaccia, Phys. Rev. E **82**, 026105 (2010).
[35] O. Gendelman, P. K. Jaiswal, I. Procaccia, B. S. Gupta, and J. Zylberg, Europhys. Lett. **109**, 16002 (2015).
[36] K. Binder and D. P. Landau, Phys. Rev. B **30**, 1477 (1984).
[37] P. Urbani and F. Zamponi, Phys. Rev. Lett. **118**, 038001 (2017).
[38] S. K. Nandi, G. Biroli, and G. Tarjus, Phys. Rev. Lett. **116**, 145701 (2016).
[39] J. Zinn-Justin, *Quantum Field Theory and Critical Phenomena* (Oxford University Press, Oxford, 2002).
[40] C. De Dominicis, I. Kondor, and T. Temesvári, *Spin Glasses and Random Fields* (World Scientific, Singapore, 1998), pp. 119–160.
[41] C. Rainone and P. Urbani, J. Stat. Mech.: Theory Exp. (2016) 053302.
[42] P. Charbonneau, J. Kurchan, G. Parisi, P. Urbani, and F. Zamponi, Nat. Comm. **5**, 3725 (2014).
[43] M. Baity-Jesi, R. A. Baños, A. Cruz, L. A. Fernandez, J. M. Gil-Narvion, A. Gordillo-Guerrero, D. Iñiguez, A. Maiorano, F. Mantovani, E. Marinari, V. Martin-Mayor, J. Monforte-Garcia, A. M. Sudupe, D. Navarro, G. Parisi, S. Perez-Gaviro, M. Pivanti, F. Ricci-Tersenghi, J. J. Ruiz-Lorenzo, S. F. Schifano, B. Seoane, A. Tarancon, R. Tripiccione, and D. Yllanes, J. Stat. Mech.: Theory Exp. (2014) P05014.
[44] M. Baity-Jesi, R. A. Baños, A. Cruz, L. A. Fernandez, J. M. Gil-Narvion, A. Gordillo-Guerrero, D. Iñiguez, A. Maiorano, F. Mantovani, E. Marinari, V. Martin-Mayor, J. Monforte-Garcia, A. Muñoz Sudupe, D. Navarro, G. Parisi, S. Perez-Gaviro, M. Pivanti, F. Ricci-Tersenghi, J. J. Ruiz-Lorenzo, S. F. Schifano, B. Seoane, A. Tarancon, R. Tripiccione, and D. Yllanes (Janus Collaboration), Phys. Rev. E **89**, 032140 (2014).

[45] L. Berthier, P. Charbonneau, Y. Jin, G. Parisi, B. Seoane, and F. Zamponi, Proc. Natl. Acad. Sci. USA **113**, 8397 (2016).
[46] J. Ashwin, O. Gendelman, I. Procaccia, and C. Shor, Phys. Rev. E **88**, 022310 (2013).
[47] G. P. Shrivastav, P. Chaudhuri, and J. Horbach, J. Rheol. (1978-present) **60**, 835 (2016).
[48] J. Kurchan, G. Parisi, and F. Zamponi, J. Stat. Mech.: Theory Exp. (2012) P10012.
[49] C. M. Bender and S. A. Orszag, *Advanced Mathematical Methods for Scientists and Engineers I* (Springer Science & Business Media, Berlin, 1999).
[50] C. Rainone, arXiv:1411.3941.
[51] A. Crisanti and H.-J. Sommers, Zeitschr. Phys. B **87**, 341 (1992).
[52] A. Bray and M. Moore, J. Phys. C **12**, 79 (1979).
[53] F. Zamponi, arXiv:1008.4844.